

Polymeric Nanoparticles Integrated from Discrete Organoplatinum(II) Metallacycle by Stepwise Post-assembly Polymerization for Synergistic Cancer Therapy

Jiong Zhou, Guocan Yu,* Jie Yang, Bingbing Shi, Boyong Ye, Mengbin Wang, Feihe Huang,* and Peter J. Stang*



Cite This: *Chem. Mater.* 2020, 32, 4564–4573



Read Online

ACCESS |



Metrics & More

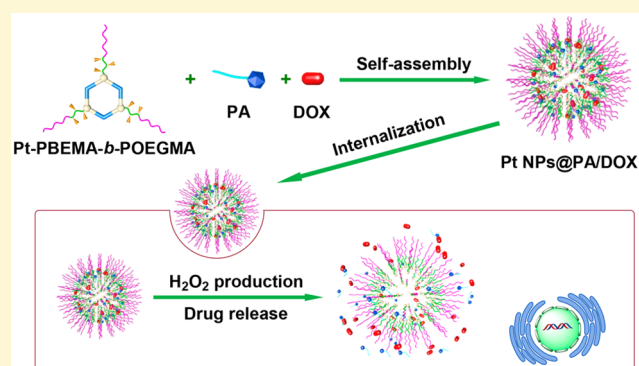


Article Recommendations



Supporting Information

ABSTRACT: Post-assembly modification is a useful tool for producing discrete metallasupramolecular structures. However, the simple structural transformation by facile covalent reactions greatly impedes the development of functional organometallic materials. Herein, we describe the successful outcome by means of coordination-driven self-assembly and post-assembly reversible addition–fragmentation chain-transfer polymerization in preparing an amphiphilic supramolecular block copolymer Pt-PBEMA-*b*-POEGMA possessing H₂O₂-responsive diblock copolymers arms and a well-defined metallacycle core. The polymer self-assembles into nanoparticles (Pt NPs), which are able to encapsulate palmitoyl ascorbate (PA) and doxorubicin (DOX). After being internalized by cancer cells, PA serves as a prooxidant to elevate the H₂O₂ concentration through cascade reactions to reverse the amphiphilicity of Pt-PBEMA-*b*-POEGMA through a H₂O₂-responsive removal of the hydrophobic domains, thus promoting the release of DOX. Meanwhile, the released quinone methide depletes the intracellular glutathione to decrease the antioxidation ability of cancer cells, realizing synergistic anticancer efficacy. Due to the sophisticated design and the enhanced permeability and retention effect, the nanomedicine codelivering PA and DOX highly accumulates in the tumor site. In vitro and in vivo results show the excellent antitumor performance of Pt NPs@PA/DOX, which greatly suppresses tumor growth after intravenous administration with negligible systemic toxicity.



INTRODUCTION

Over the past few decades, coordination-driven self-assembly has grown into a potent synthetic method to produce discrete supramolecular coordination complexes (SCCs) with specific shapes, sizes, and geometries.^{1–7} Many exquisite two-dimensional metallacycles and three-dimensional metallacages have been exploited by the advisable choice of ligands and metals.^{8–15} These metallasupramolecular structures are especially attractive because of their esthetical characteristics and extensive applications in the fields of sensors, supramolecular polymers, host–guest chemistry, amphiphilic self-assembly, and drug delivery.^{16–28} In order to exploit new multifunctional organometallic materials, recent works have focused on the derivatization of metallasupramolecular architectures.^{29–31}

Post-assembly modification has been extensively used in adjusting the functionalities and formation of biomedical superstructures.^{32,33} Enlightened by many successful examples of post-assembly modification in biomedical systems, such modification of supramolecular species has been widely exploited in domains such as covalently modified poly-

mers,^{34,35} mechanically interlocked structures,^{36–40} and metal–organic frameworks.^{41,42} This approach enables one to adjust the architecture of supramolecular ensembles, resulting in the higher degree of complexity and diverse functionality.⁴³ Controlled radical polymerization has been widely used in constructing functional polymers,⁴⁴ which provides an easy method to produce polymeric materials with desired functions and well-defined architectures. The stability of intact SCCs under physiological conditions is required to be enhanced for biomedical applications.⁴⁵ The low tumor accumulation and poor solubility of SCCs are two other main barriers.⁴⁶ Encapsulation by polymers and chemical functionalization of SCCs are feasible methods to resolve such

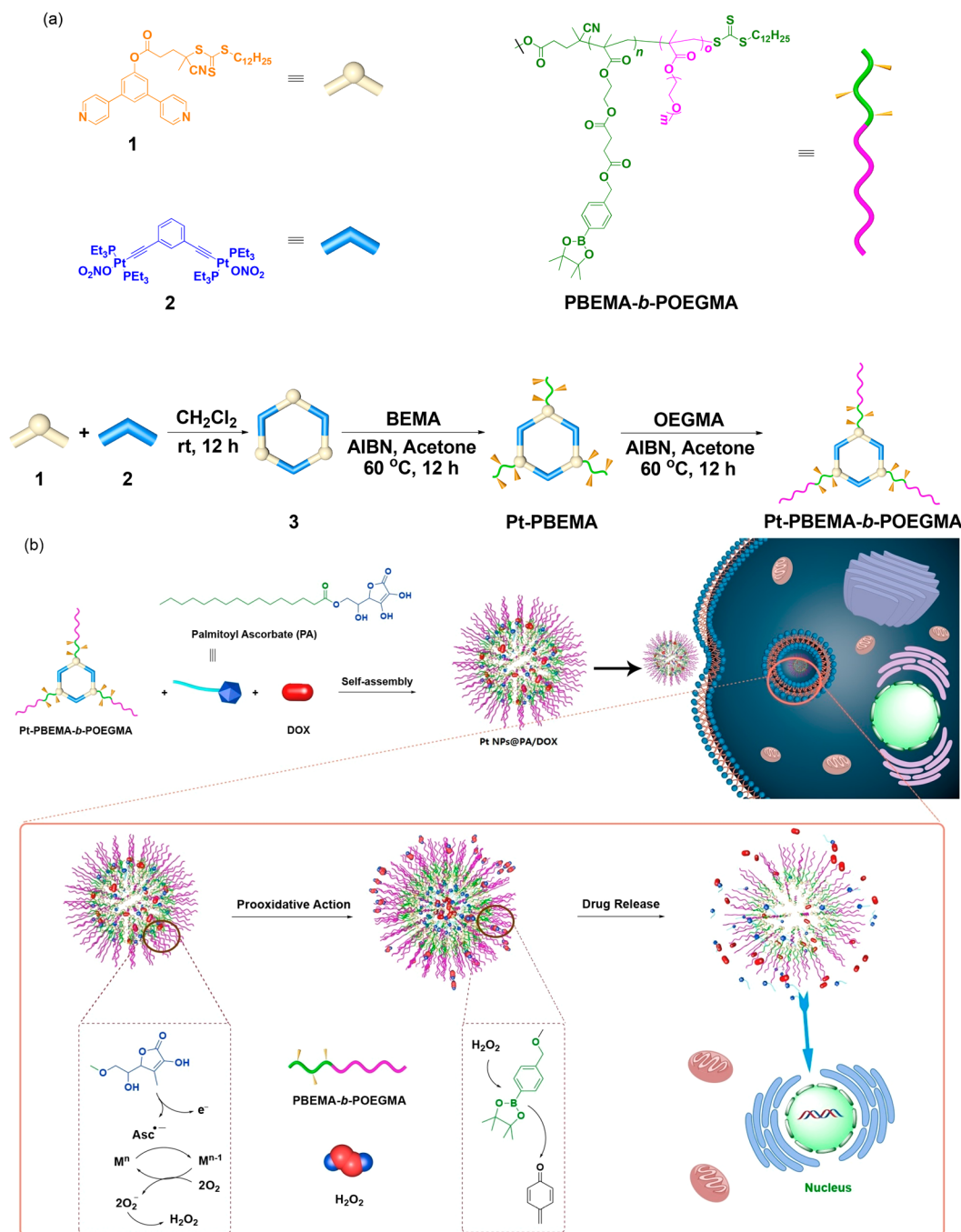
Received: February 12, 2020

Revised: May 14, 2020

Published: May 15, 2020



Scheme 1. (a) Graphic Presentation of the Preparation of Organoplatinum(II) Metallacycle and Supramolecular Block Copolymer; (b) Schematic Illustration of Integrated Polymeric Nanoparticles Self-Assembled from Pt-PBEMA-*b*-POEGMA as H₂O₂-Responsive Drug Delivery Vehicles



issues.⁴⁷ In particular, post-assembly modification of SCCs by amphiphilic copolymers is an effective way to fabricate drug delivery systems (DDSs), since the strategy enhances the stability and the solubility of SCCs and also enables anticancer drugs to be loaded into the polymer scaffold, realizing synergistic anticancer activity.^{48,49} Besides, stimuli responsiveness is able to be introduced to increase treatment efficacy and to reduce adverse side effects.^{50–53}

Herein, we successfully combine the coordination-driven self-assembly and post-assembly reversible addition–fragmentation chain-transfer (RAFT) polymerization to prepare an amphiphilic copolymer Pt-PBEMA-*b*-POEGMA with H₂O₂-

responsive diblock copolymers arms and a well-defined metallacycle core (Scheme 1). The polymer self-assembles into nanoparticles (Pt NPs) via a reprecipitation technique, and the obtained Pt NPs are able to encapsulate hydrophobic doxorubicin (DOX) and palmitoyl ascorbate (PA). Because of the enhanced permeability and retention (EPR) effect and the nanoformulation, high tumor accumulation and a long circulation time of the nanomedicine is realized, which are favorable for cancer treatment.^{54,55} The loaded PA serves as a prooxidant to elevate the intracellular H₂O₂ concentration to cleave the hydrophobic protection groups through a H₂O₂-triggered cascade elimination reaction. The amphiphilic

property of copolymer Pt-PBEMA-*b*-POEGMA is reversed, leading to the disruption of nanoarchitectures and subsequent release of loaded drugs. More interestingly, the resealed quinone methide (QM) effectively depletes the intracellular glutathione (GSH) to reduce the antioxidative capacity of cancer cells, promoting the anticancer efficacy of this potential nanomedicine. In vivo evaluations demonstrate that the excellent antitumor outcomes combine the chemotherapy and amplification of oxidative stress in a synergistic manner.

EXPERIMENTAL SECTION

Materials and Methods. Poly(ethylene glycol) methacrylate (OEGMA, $M_n = 500$) and other reagents were purchased from Sigma-Aldrich. Solvents were dried according to the literature. NMR spectra were recorded on a Bruker Avance III-400 spectrometer with internal standard TMS. $^{31}\text{P}\{^1\text{H}\}$ NMR chemical shifts were referenced to an external unlocked sample of 85% H_3PO_4 ($\delta = 0.0$). High-resolution mass spectrometry experiments were carried out by a Bruker 7-T FT-ICR mass spectrometer equipped with an electrospray source (Billerica, MA, USA). The fluorescence experiments were conducted on a Horiba Fluoromax-4 spectrometer. Transmission electron microscopy (TEM) studies were performed on a Jeol JEM 2010 apparatus. The fluorescence tests were conducted on a RF-5301 spectrofluorophotometer (Shimadzu Corp., Japan). Dynamic light scattering (DLS) experiments were conducted on a 200 mW polarized laser source Nd:YAG ($\lambda = 532$ nm).

Preparation of PA-Loaded Pt NPs (Pt NPs@PA) and DOX-Loaded Pt NPs (Pt NPs@DOX). For drug loading, neutral DOX was used by deprotonating the cationic drug. Briefly, cationic DOX (20.0 mg) was solubilized in a mixture of distilled water (5 mL) and tetrahydrofuran (5 mL), 1 drop of triethylamine was added, and the solution was stirred for 15 min. Then the organic phase was removed by rotary vacuum. The formed precipitate was collected through centrifugation and dried in vacuum for further use. Pt NPs@PA (or Pt NPs@DOX) were obtained through a reprecipitation method. Briefly, Pt-PBEMA-*b*-POEGMA or Pt-PBrEMA-*b*-POEGMA (100 mg) and PA (or DOX, 40.0 mg) were dissolved in 30 mL of tetrahydrofuran, and the solution was gradually injected into 250 mL of Milli-Q water under sonication. After stirring overnight at room temperature to evaporate the tetrahydrofuran, the mixture was sealed in a dialysis bag with a molecular weight cutoff of 3 kDa and dialyzed against DI water for 2 h to remove unloaded drugs. The same method was utilized for the preparation of Pt NPs@PA/DOX (*n* Pt NPs@PA/DOX). The mass of Pt-PBEMA-*b*-POEGMA (or Pt-PBrEMA-*b*-POEGMA) was 100 mg, and the mass of the PA/DOX mixture with different ratios was 40.0 mg. Drug encapsulation was calculated using the following equation

$$\text{drug-loading content (\%)} = \left[\frac{m_{\text{drug-loaded}}}{(m_{\text{polymer}} + m_{\text{drug-loaded}})} \right] \times 100$$

where $m_{\text{drug-loaded}}$ and m_{polymer} are the masses of the encapsulated drug in the nanostructures and the polymer, respectively.

Transmission Electron Microscopy (TEM) and Dynamic Light Scattering (DLS) Studies. The morphology of the nanoformulations was revealed using TEM. TEM samples were made by drop coating the corresponding solution onto the carbon-coated copper grid. The size and stability of Pt NPs@PA/DOX was confirmed by measuring their mean diameters after different periods of incubation by DLS tests.

Cell Culture. HeLa cells were purchased from American Type Culture Collection (ATCC, Rockville MD) and incubated in Dulbecco's MEM (DMEM) supplemented with fetal bovine serum (10%) and penicillin/streptomycin (1%). The cells grew in a single layer and were isolated by trypsin after fusion (0.5% phosphate-buffered saline). After being extracted from culture medium and incubated in the trypsin solution for 5 min, the cells were centrifuged and the supernatant was removed. Then 3.00 mL of serum-containing

DMEM was added to neutralize the remaining trypsin. Cells were then resuspended in serum-containing DMEM at a concentration of 1.00×10^4 cells/mL and incubated in 37 °C and 5% CO_2 .

Evaluation of Cytotoxicity. The cytotoxicity against HeLa cells was evaluated by a 3-(4,5-dimethylthiazol-2-yl)-2,5-diphenyltetrazolium bromide (MTT) assay. All solutions were uniformly sterilized by a 0.22 μm filter before testing. HeLa cells were seeded in 96-well plates with a density of 1.00×10^4 cells/well and cultured for 24 h. The cells were then cultured with PA, DOX, Pt NPs@PA, Pt NPs@DOX, Pt NPs@PA/DOX, and *n* Pt NPs@PA/DOX at various concentrations for 48 h. After washing the cells with phosphate-buffered saline, 20 μL of MTT solution (5.00 mg/mL) was added to every well. After being cultured for 4 h at 37 °C, the medium was removed and the cells were washed with phosphate-buffered saline three times. The insoluble formazan crystals were dissolved by dimethyl sulfoxide (100 μL), and the absorbance was detected by the spectrophotometer (570 nm). Untreated cells were used as a control. Each experiment was conducted with five replicates.

In Vitro Cell Accumulation Determined by Confocal Laser Scanning Microscopy (CLSM). HeLa cells were treated with the Pt NPs@PA/DOX or *n* Pt NPs@PA/DOX (the concentration of DOX was kept at 1.00 μM) in culture medium for 4 and 8 h at 37 °C. After being washed with phosphate-buffered saline, the cells were stained with 4',6-diamidino-2-phenylindole (DAPI) and lysotracker green (200 nM). The images were taken using a LSM-510 confocal laser scanning microscope (CLSM, ZEISS LSM780).

Tumor Model. Nude mice (~ 20 g body weight, 4 weeks old) were purchased from Zhejiang Academy of Medical Sciences and kept under controlled temperature (24 °C) in the pathogen-free environment. Research involving animals was approved by the Animal Protection and Utilization Committee of Zhejiang University. Nude mice were subcutaneously injected with cell suspension (200 μL , 5×10^6 HeLa cells) at the right flank region. The formula of (tumor length) \times (tumor width) $^2/2$ was used to calculate the tumor volume.

Pharmacokinetics and Tissue Distributions. Mice received DOX (5.00 mg/kg) or Pt NPs@PA/DOX (5.00 mg DOX/kg) through tail mainline. The blood was collected and stored in a heparinized tube. The lung, liver, kidney, spleen, and tumor were removed after intravenous injection for 24 h and stored in dry ice before analysis. The viscera were digested, and DOX was quantitatively analyzed through HPLC.

In Vivo Antitumor Activity. Tumor volume and body weights were measured for individual animals in all experiments. The mice were randomly divided into five treatment groups ($n = 5$), and the average tumor volume was about 100 mm^3 . The mice were injected intravenously with PBS, DOX (5.00 mg/kg), Pt NPs@PA, Pt NPs@DOX (5.00 mg DOX/kg), *n* Pt NPs@PA/DOX (5.00 mg DOX/kg), or Pt NPs@PA/DOX (5.00 mg DOX/kg) every 3 days three times. Body weight and tumor volume were measured every 3 days.

Synthesis of Hexagonal Metallacycle 3. Compounds 1 (12.7 mg, 20.0 μmol) and 2 (22.2 mg, 20.0 μmol) were placed in a 20 mL glass ampule. About 5 mL of dichloromethane was added; the glass ampule was sealed and stirred for 12 h at room temperature. The solvent was removed, and diethyl ether was slowly added to precipitate product 3 as a light yellow powder (31.4 mg, 90%).

Synthesis of Supramolecular Polymer Pt-PBEMA. Supramolecular hexagonal metallacycle 3 (8.00 μmol), AIBN (0.800 μmol), and [2-(((4-(4,4,5,5-tetramethyl-1,3,2-dioxaborolan-2-yl)benzyl)-oxy)carbonyl)oxy]ethyl methacrylate] (BEMA) (0.400 μmol) were placed in a 10.0 mL glass ampule. About 1.5 mL of acetone was added. The mixed solution was degassed via three cycles of freeze-pump-thawing and then transferred to an oil bath at 60 °C to start polymerization. Twelve hours later, the polymerization reaction was stopped with liquid nitrogen. The resulting mixture was precipitated with cold diethyl ether. The residues were dissolved in acetone again and precipitated with cold diethyl ether. The product was dried overnight under reduced pressure at room temperature.

Synthesis of Supramolecular Block Copolymer Pt-PBEMA-*b*-POEGMA. Supramolecular polymer Pt-PBEMA (5.00 μmol),

AIBN (0.500 μmol), and OEGMA (250 μmol) were placed in a 10.0 mL glass ampule. About 1.5 mL of acetone was added. The mixed solution was degassed via three cycles of freeze–pump–thawing and then transferred to an oil bath at 60 $^{\circ}\text{C}$ to start polymerization. Eight hours later, the polymerization reaction was stopped with liquid nitrogen. The resulting mixture was precipitated with cold diethyl ether. The residues were dissolved in acetone again and precipitated with cold diethyl ether. The product was dried overnight under reduced pressure at room temperature, resulting in a light yellow oil.

RESULTS AND DISCUSSION

Preparation of Supramolecular Block Copolymers Possessing Hexagonal Metallacycle via Stepwise Post-assembly Polymerization. To construct a functionalized supramolecular block copolymer possessing a well-defined discrete metallacycle core, BEMA was selected as a H_2O_2 -responsive monomer in constructing oxidation-responsive materials.^{56,57} Treatment of H_2O_2 triggered the degradation of boronate ester to release QM, which is proved to react with GSH.^{58,59} In view of the fact that GSH acts as the main reducing agent in cancer cells to keep an oxidation–reduction equilibrium, effective GSH depletion by the released QM is supposed to reduce the antioxidative capacity of cancer cells. In addition, BrEMA was selected as a control monomer due to its nonresponsiveness (Scheme S2 and Figure S4).

According to the rule of coordination-driven self-assembly, a discrete hexagonal metallacycle is formed through a combination of three 120 $^{\circ}$ organoplatinum(II) acceptors with three 120 $^{\circ}$ donor ligands. As shown in Scheme 1a, 120 $^{\circ}$ dipyrindyl ligand **1** containing a trithioester group, a traditional chain transfer agent that can be used for RAFT polymerization, was prepared. Next, self-assembly of ligand **1** with 120 $^{\circ}$ organoplatinum(II) acceptor **2** in CH_2Cl_2 gave hexagonal metallacycle **3** in an alternate way. Formation of hexagonal metallacycle **3** was clearly characterized through ^1H and $^{31}\text{P}\{^1\text{H}\}$ NMR spectra. With the hexagon **3** in hand, the block copolymer containing a metallacycle as the scaffolding was obtained through stepwise post-assembly polymerization (Scheme 1). The intermediate polymer Pt-PBEMA was synthesized by polymerizing BEMA with hexagon **3** in acetone. The reaction solution was deaerated by three cycles of a freeze–pump–thawing process, and then the polymerization reaction was conducted at 60 $^{\circ}\text{C}$ for 12 h. Pt-PBEMA was obtained by cold diethyl ether precipitation and dried overnight. Subsequently, the targeted supramolecular block copolymer Pt-PBEMA-*b*-POEGMA was eventually acquired from Pt-PBEMA by polymerizing OEGMA using the same method.

Formation of both the intermediate polymer Pt-PBEMA and the supramolecular block copolymer Pt-PBEMA-*b*-POEGMA was clearly characterized by ^1H and $^{31}\text{P}\{^1\text{H}\}$ NMR spectra. For example, the ^1H NMR spectrum of Pt-PBEMA-*b*-POEGMA showed characteristic signals of PBEMA, such as the resonance peaks at 7.36 and 7.80 ppm attributed to phenylboronic acid pinacol ester protons (Figure 1a–c). Moreover, signals at 4.28 ppm were attributed to the methylene protons in POEGMA. In general, the characterization was in the high consistence of the production of a three-armed block copolymer. Of particular note was that in comparison with the original metallacycle **3**, the peaks related to the pyridyl moieties of both Pt-PBEMA and Pt-PBEMA-*b*-POEGMA remained almost unchanged. Besides, the $^{31}\text{P}\{^1\text{H}\}$ NMR spectrum of the polymer Pt-PBEMA-*b*-POEGMA

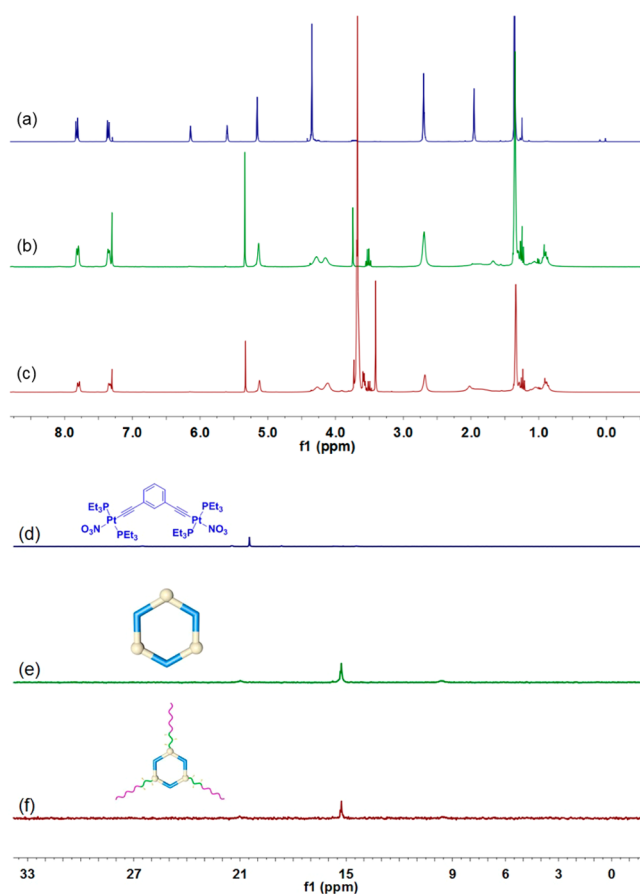


Figure 1. ^1H NMR spectra (400 MHz, CDCl_3 , 293 K) of (a) BEMA, (b) Pt-PBEMA-*b*-POEGMA, and (c) PBEMA-*b*-POEGMA. $^{31}\text{P}\{^1\text{H}\}$ NMR spectra (121.4 MHz, $\text{DMSO}-d_6$, 293 K) of (d) **2**, (e) **3**, and (f) Pt-PBEMA-*b*-POEGMA.

revealed a singlet at 15.24 ppm, which was nearly the same as that of the parent metallacycle **3** (15.27 ppm) (Figure 1d–f). The results demonstrated that the stepwise post-assembly RAFT polymerization generated a new supramolecular block copolymer with a well-defined metallacycle core.

Preparation of the NPs as Dual-Responsive Drug Delivery Vehicles. Through a fluorescent approach, the critical aggregation concentration (CAC) of the amphiphilic polymer Pt-PBEMA-*b*-POEGMA was measured to be 4.94 $\mu\text{g}/\text{mL}$ (Figure 2a), which was much lower than that of the disassembled polymer PBEMA-*b*-POEGMA with a CAC value of 40.3 $\mu\text{g}/\text{mL}$ (Figure S18), suggesting that formation of metallacycle increased the stability of the amphiphilic polymer. The metallacycle linked by the coordination interaction served as the cross-linker to stabilize the nanocarriers to avoid leakage of drugs, illuminating the important role of this metallacycle in drug delivery.

The PA-loaded Pt NPs (Pt NPs@PA) and DOX-loaded Pt NPs (Pt NPs@DOX) were prepared from Pt-PBEMA-*b*-POEGMA by the coassembly technique with a high loading efficiency (Table S1). Besides, the hydrophobic agents PA and DOX could be coencapsulated by Pt-PBEMA-*b*-POEGMA using the same method. When changing the ratio of PA/DOX from 8:1 to 1:8, the drug-loading efficiency remained almost unchanged (Figure S19). However, a slight change in diameter was detected by DLS measurements when changing the ratio of PA/DOX from 8:1 to 1:8 (Figure 2b). van der Waals force

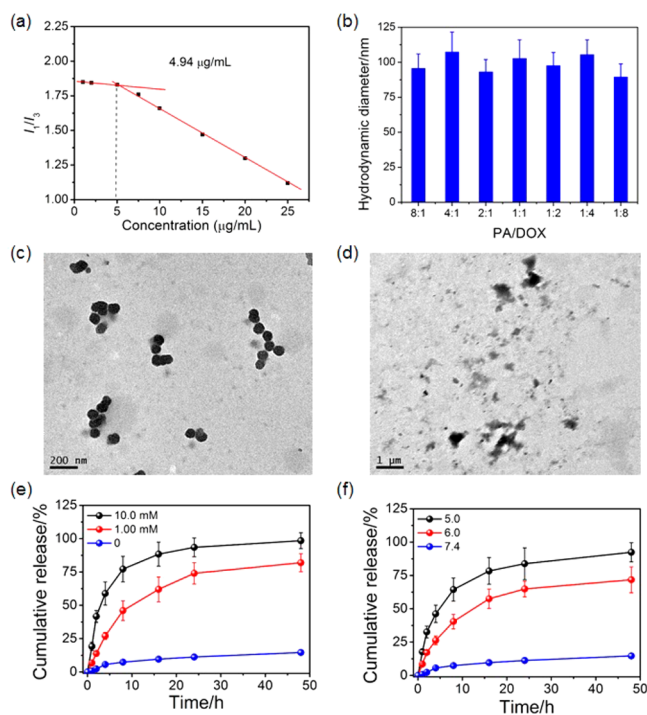


Figure 2. (a) CAC measurement of Pt-PBEMA-*b*-POEGMA using pyrene as a probe. (b) Average diameters of Pt NPs@PA/DOX with different PA/DOX ratios. TEM images of (c) Pt NPs@PA/DOX (PA/DOX = 1:4) and (d) Pt NPs@PA/DOX after H₂O₂ treatment. (e) Drug release curves of DOX from Pt NPs@PA/DOX with or without different concentrations of H₂O₂. (f) Drug release curves of DOX from Pt NPs@PA/DOX at different pH values.

and π - π stacking interactions are the main driving forces for PA and DOX to be encapsulated by the amphiphilic Pt-PBEMA-*b*-POEGMA. To find the optimized ratio between PA and DOX for in vivo and in vitro studies, a synergistic effect was investigated by MTT assay. As shown in Figure S24, the anticancer efficacy was the most potent at a PA/DOX ratio of 1:4. Therefore, this optimized ratio was employed for the preparation of Pt NPs@PA/DOX for further investigations. The morphology of the resultant nanomedicine was revealed by TEM, in which nanoparticles with diameters of 80–120 nm were observed (Figure 2c). Importantly, Pt NPs@PA/DOX was stable in PBS possessing 10% FBS over a period of 2 days (Figure S20), verifying the high colloidal stability of Pt NPs@PA/DOX in biological buffer.

Pharmacologic PA can act as a prooxidant to produce H₂O₂ through cascade reactions inside cells.^{60,61} The elevated concentration of H₂O₂ triggered the disassembly of Pt NPs@PA/DOX to get the loaded drug released. The release behavior was assessed by a dialysis approach at different concentrations of H₂O₂. In the absence of H₂O₂, only 14.6% DOX was released within 48 h (Figure 2e). However, 82.0% and 98.5% DOX were released at 1.00 and 10.0 mM of H₂O₂ at the same time scale due to H₂O₂-triggered decomposition of Pt NPs@PA/DOX. A similar release behavior of PA from Pt NPs@PA/DOX was observed, indicating that the dual drugs could be effectively released after cellular internalization (Figure S21). The original state of DOX encapsulated in the assembly of the Pt NPs@PA/DOX is neutral, but in intracellular acidic environment, it changes to the cationic state because of protonation, thereby accelerating its release. The release progress of DOX from Pt NPs@PA/DOX was

also performed at different pH, simulating the pH gradient existing between the endosomal and the lysosomal compartments. As indicated in Figure 2f, the DOX release curve was obviously pH dependent; 71.8% of DOX was released from Pt NPs@PA/DOX after 48 h at pH 6.0 and 92.4% at pH 5.0.

The H₂O₂ responsiveness of the nanomedicine was further validated using ¹H NMR spectroscopy. In the ¹H NMR spectrum of Pt-PBEMA-*b*-POEGMA, signals related to the protons of BEMA moieties ranging from 7.29 to 7.65 ppm completely vanished by culturing the solution with H₂O₂ (1.00 mM) for 5 min (Figure S22), indicating a thorough elimination was achieved. TEM images showed that Pt NPs@PA/DOX changed to irregular assemblies after H₂O₂ treatment, suggesting the disassembly of the nanomedicine (Figure 2d).

By making use of the intrinsic fluorescence of DOX, CLSM was utilized to study the internalization of Pt NPs@PA/DOX. The red fluorescence color of DOX was found mainly in the cytoplasm and overlapped well with the green signal from lysosome tracker (Figure 3, a and b). DOX was released via disassembly of Pt NPs@PA/DOX and then accumulated in the nucleus. It should be noted that in the CLSM image, the breakdown of the cell nucleus was clearly monitored for cells treated with Pt NPs@PA/DOX for 24 h, one of the hallmarks of apoptosis. In sharp contrast, a small amount of DOX was released from nonresponsive nanomedicine (*n* Pt NPs@PA/DOX) prepared from Pt-PBEMA-*b*-POEGMA due to the shortage of responsiveness. The red fluorescence stayed in the cytoplasm even after 8 h of incubation (Figure S23). These studies revealed that Pt NPs@PA/DOX could be effectively internalized by cancer cells and released the loaded therapeutic agents.

Interestingly, the released PA served as a prooxidant to elevate the intracellular H₂O₂ concentration, further boosting the drug release. The produced QM from Pt NPs@PA also reduced the antioxidative capacity of cancer cells through GSH depletion, thus improving the intracellular oxidative stress. In order to study the intracellular reactive oxygen species (ROS) elevation in HeLa cells, DCFH-DA was utilized as a fluorimetric marker to detect the intracellular ROS. The cells treated with PBS or Pt NPs revealed weak fluorescence, which was ascribed the intrinsic ROS degree inside cells (Figure 3c). By comparison, the cells treated with PA and Pt NPs@PA greatly promoted the intracellular ROS concentration. Figure 3d shows that about 4-fold enhancement in the ROS degree is achieved for the cells incubated with Pt NPs@PA, which is much higher than that of free PA. A possible reason is that the endocytosis of PA is increased by blocking its negative charge upon formation of the nanomedicine. The ROS signal was remarkably diminished by pretreating the cells with a ROS scavenger (sodium ascorbate, NaVC) followed by incubation of Pt NPs@PA. To assess the GSH-depleting capacity of Pt NPs@PA, the GSH content in HeLa cells after treatment with Pt NPs@PA was further studied through a GSH/GSSG detection kit. After dealing with different contents of Pt NPs@PA, the amount of GSH was quantitatively determined. As indicated in Figure 3e, treatment with Pt NPs@PA reduced the intracellular GSH degree to be lower than 50% of the original one. Therefore, the effective GSH depletion capacity of Pt-PBEMA-*b*-POEGMA polymer presumably produces this result.

The anticancer efficacies of DOX, PA, Pt NPs@PA, Pt NPs@DOX, *n* Pt NPs@PA/DOX, and Pt NPs@PA/DOX

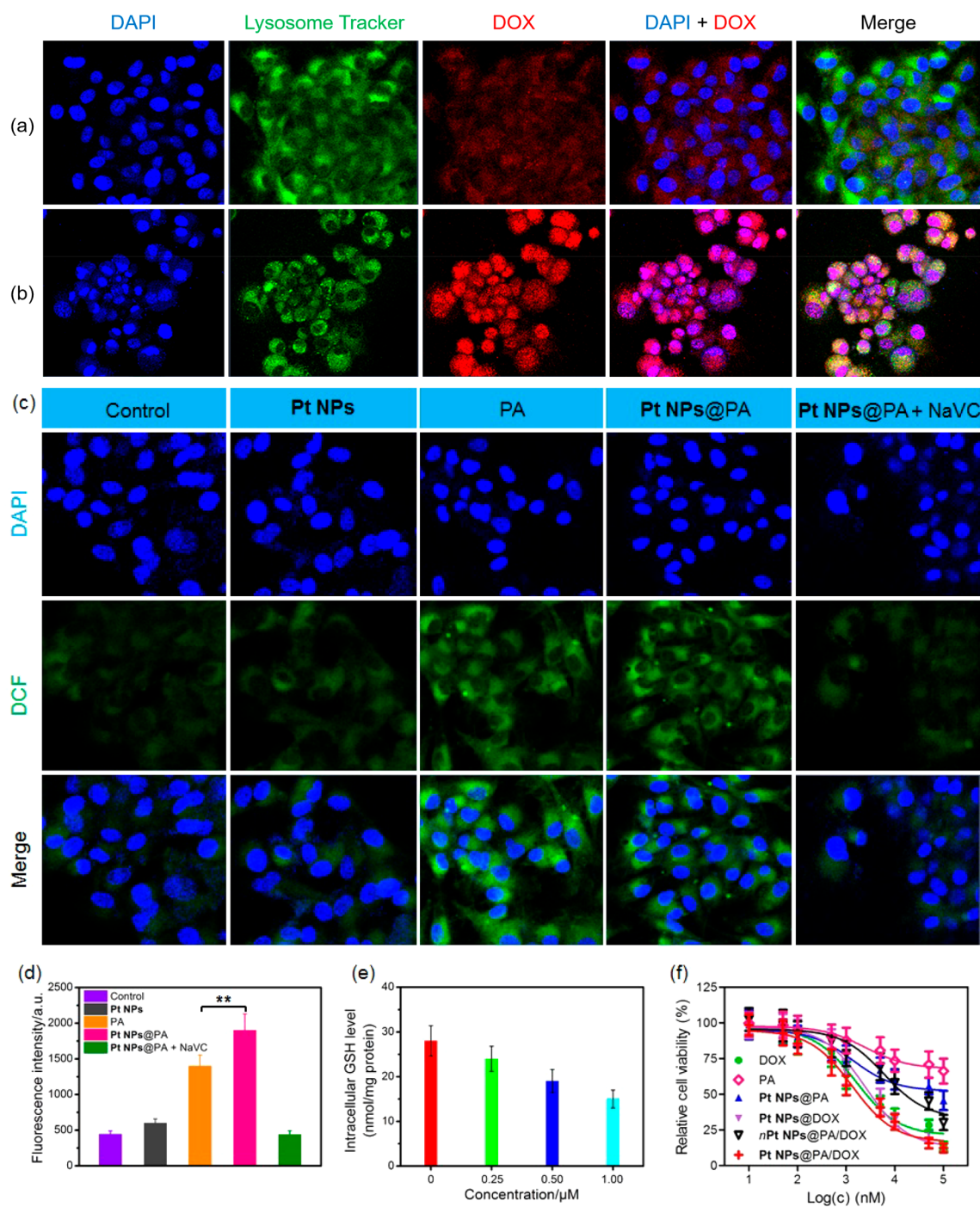


Figure 3. CLSM images of the HeLa cells incubated with Pt NPs@DOX for (a) 4 and (b) 8 h. (c) CLSM images of the ROS degree inside HeLa cells after treatment under different conditions using DCFH-DA as a ROS probe. (d) Fluorescence intensity of the ROS signal was quantified from c. $**p < 0.01$. Results are expressed as mean \pm s.d. (e) GSH degree after treatment with various concentrations of Pt NPs@PA in HeLa cells. (f) Cytotoxicity of DOX, PA, Pt NPs@PA, Pt NPs@DOX, nPt NPs@PA/DOX, and Pt NPs@PA/DOX against HeLa cells after 48 h incubation.

were evaluated using a MTT assay (Figure 3f). Compared with free PA, the cytotoxicity of Pt NPs@PA was greatly enhanced because of the favorable cellular uptake and effective release by formation of this nanoformulation. The half-maximal inhibitory concentrations (IC_{50}) of Pt NPs@DOX was calculated to be $2.48 \pm 0.27 \mu\text{M}$, which was comparable to that of free DOX ($IC_{50} = 1.63 \pm 0.21 \mu\text{M}$), proving the anticancer capability of Pt NPs@DOX was kept. More importantly, the anticancer efficacy of Pt NPs@PA/DOX was promoted by codelivering PA and DOX; the IC_{50} value decreased to $1.32 \pm 0.16 \mu\text{M}$. It

should be stressed that the cytotoxicity of the nanoformulations prepared from the nonresponsive copolymer was much lower than those fabricated from Pt-PBEMA-*b*-POEGMA, indicating the H_2O_2 responsiveness played an important role in cancer therapy.

In Vivo Drug Delivery and Cancer Therapy. Nanosized agents with proper diameters preferentially accumulate in tumors through the permeable tumor vessel and are retained in the tumor bed because of reduced lymphatic drainage.^{62–64} Besides, the PEG groups on the exterior of Pt NPs can protect

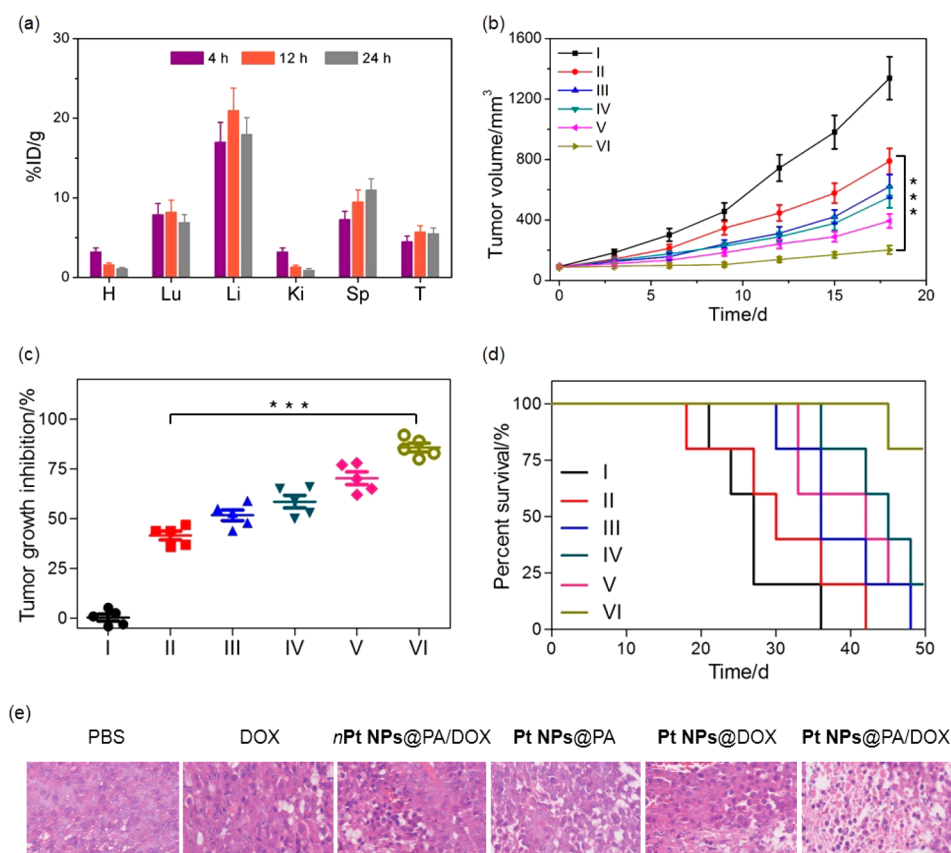


Figure 4. (a) Tissue distribution of Pt NPs@PA/DOX in the main organs and tumor at different postinjection times. H, heart; Lu, lung; Li, liver; Ki, kidney; Sp, spleen; T, tumor. (b) Tumor growth curves, (c) inhibition rate, and (d) survival rate of the mice with HeLa tumors after different treatments. I, PBS; II, DOX; III, *n* Pt NPs@PA/DOX; IV, Pt NPs@PA; V, Pt NPs@DOX; VI, Pt NPs@PA/DOX. *** $p < 0.001$. (e) H&E analysis of tumor tissues after different formulations.

them against being absorbed by proteins and eliminated from the body. The pharmacokinetic behaviors of Pt NPs@PA/DOX and free DOX were evaluated (Figure S27). Compared with DOX that was rapidly cleared out from the body, the circulation time of Pt NPs@PA/DOX was significantly prolonged. After intravenous injection of Pt NPs@PA/DOX for 24 h, about 1.5% ID/g blood can be measured. Furthermore, the time-dependent biodistribution of Pt NPs@PA/DOX in the main organs and tumor was quantitatively analyzed (Figure 4a). In the case of free DOX, the tumor accumulation was very low because of its fast clearance and nonspecific distribution (Figure S28). Benefiting from the EPR effect, the DOX amount in the tumor after treatment with Pt NPs@PA/DOX gradually increased to $5.7 \pm 0.8\%$ ID/g after 12 h postinjection. The intratumoral DOX amount remained at a high degree ($5.5 \pm 0.7\%$ ID/g) even at 24 h postinjection, which facilitated its antitumor performance. In addition, the biodistribution of Pt NPs@PA/DOX in the main organs was comparable to free DOX, while the relatively slow release was favorable to change the excretion behaviors and reduce its systemic toxicity.

To assess the *in vivo* antitumor effect, six groups of mice with HeLa tumor were injected intravenously by PBS, DOX, *n* Pt NPs@PA/DOX, Pt NPs@PA, Pt NPs@DOX, and Pt NPs@PA/DOX. The tumors exhibited an exponential growth pattern with time and showed a mean tumor volume of 1350 mm^3 for the mice cultured by PBS after 18 days (Figure 4b). In the DOX-treated formulation, a moderate inhibition of tumor growth was accomplished with a mean tumor volume of 795

mm^3 at the same period. Due to the EPR effect and H_2O_2 -responsive drug release, Pt NPs@DOX and Pt NPs@PA showed better antitumor efficacy compared with free DOX. Specifically, the Pt NPs@PA/DOX group greatly outperformed other groups in diminishing the volume of the tumors as a result of the synergistic anticancer efficacy. After the final injection, the mice were sacrificed and the tumors were removed and weighed individually. Consequently, the inhibition rates of tumor growth were measured to be 41.6%, 51.8%, 58.6%, 70.4%, and 85.8% for the mice administrated with DOX, *n* Pt NPs@PA/DOX, Pt NPs@PA, Pt NPs@DOX, and Pt NPs@PA/DOX, respectively (Figure 4c), further demonstrating the best therapeutic efficacy of Pt NPs@PA/DOX. The antitumor effect was also evaluated using hematoxylin/eosin (H&E) staining. In these treatment formulations, the tumor tissues showed the lowest proliferation of cells and the highest degree of necrosis after treatment with Pt NPs@PA/DOX, demonstrating massive remission of the proliferation activity (Figure 4e).

To evaluate the systemic toxicity of Pt NPs@PA/DOX, the impact of diverse groups upon body weight, survival rate, and blood chemistry was studied. For free DOX, the body weight of mice decreased during the period of drug administration due to the side effect of DOX. On the contrary, there was no obvious body weight loss after treatment with Pt NPs@PA/DOX, proving that the systemic toxicity was negligible using this nanoformulation (Figure S29). Compared to other groups (27, 30, 37.5, 36, and 45 days for PBS, DOX, Pt NPs@PA/DOX, Pt NPs@PA, and Pt NPs@DOX, respectively), the

average lifespan of mice after treatment with Pt NPs@PA/DOX was greatly prolonged (Figure 4d), owing to its negligible systemic toxicity and outstanding antitumor performance. Besides, blood biochemistry was performed at 1, 4, and 7 days postadministration of Pt NPs@PA/DOX to evaluate the hepatotoxicity and nephrotoxicity (Figures S30–34). These mice revealed the same regular parameters with mice that had not been treated, further showing that neither liver damage nor renal dysfunction was led by Pt NPs@PA/DOX.

CONCLUSION

In summary, we developed a new supramolecular block copolymer Pt-PBEMA-*b*-POEGMA consisting of a well-defined metallacycle core and three H₂O₂-responsive diblock copolymers arms by combining coordination-driven self-assembly and stepwise post-assembly polymerization. Using the reprecipitation approach, self-assemblies of Pt NPs were successfully prepared from this amphiphilic polymer. Furthermore, Pt NPs were able to encapsulate PA and DOX. In tumor tissues, the elevated level of PA served as a prooxidant and produced more H₂O₂. In the meantime, PBEMA segments generated QM responding to the high content of H₂O₂, which consumed intracellular GSH to decrease the antioxidant ability of cancer cells. The amphiphilic property of polymer Pt-PBEMA-*b*-POEGMA was changed by a H₂O₂-responsive removal of the hydrophobic domains, leading to the disruption of nanoarchitectures and subsequent release of drugs. In vitro and in vivo results revealed the excellent antitumor efficiency of Pt NPs@PA/DOX by combining the chemotherapy and amplification of oxidative stress in a synergistic manner. Although several nanomedicines have been approved by the FDA for clinic use and their side effects of the chemotherapy can be attenuated by exploiting nanotechnology, the antitumor performances are marginally improved compared with the free drugs. Different from the commercial nanomedicines prepared from liposomes, such as Doxil and Onivyde, Pt-PBEMA-*b*-POEGMA used as a drug carrier could deplete the intracellular GSH to further boost the anticancer efficacy. Another advantage of this nanomedicine was that controlled drug release could be achieved by the elevated GSH level in cancer cells, which was favorable to improve the anticancer efficacy while avoiding side effects. In view of these results, the study offers a valuable methodology and information for the reasonable design of new drug delivery systems based on supramolecular ensembles.

ASSOCIATED CONTENT

Supporting Information

The Supporting Information is available free of charge at <https://pubs.acs.org/doi/10.1021/acs.chemmater.0c00615>.

Experimental details, NMR spectra, and other materials (PDF)

AUTHOR INFORMATION

Corresponding Authors

Guocan Yu – Laboratory of Molecular Imaging and Nanomedicine, National Institute of Biomedical Imaging and Bioengineering, National Institutes of Health, Bethesda, Maryland 20892, United States; Email: guocan.yu@nih.gov
Feihe Huang – State Key Laboratory of Chemical Engineering, Center for Chemistry of High-Performance & and Novel

Materials, Department of Chemistry, Zhejiang University, Hangzhou 310027, People's Republic of China; Green Catalysis Center and College of Chemistry, Zhengzhou University, Zhengzhou 450001, People's Republic of China; orcid.org/0000-0003-3177-6744; Email: fhuang@zju.edu.cn

Peter J. Stang – Department of Chemistry, University of Utah, Salt Lake City, Utah 84112, United States; orcid.org/0000-0002-2307-0576; Email: stang@chem.utah.edu

Authors

Jiong Zhou – State Key Laboratory of Chemical Engineering, Center for Chemistry of High-Performance & and Novel Materials, Department of Chemistry, Zhejiang University, Hangzhou 310027, People's Republic of China; orcid.org/0000-0002-3916-0189

Jie Yang – State Key Laboratory of Chemical Engineering, Center for Chemistry of High-Performance & and Novel Materials, Department of Chemistry, Zhejiang University, Hangzhou 310027, People's Republic of China; orcid.org/0000-0001-9970-7505

Bingbing Shi – Department of Chemistry, University of Utah, Salt Lake City, Utah 84112, United States; orcid.org/0000-0001-9523-5758

Boyong Ye – State Key Laboratory of Chemical Engineering, Center for Chemistry of High-Performance & and Novel Materials, Department of Chemistry, Zhejiang University, Hangzhou 310027, People's Republic of China

Mengbin Wang – State Key Laboratory of Chemical Engineering, Center for Chemistry of High-Performance & and Novel Materials, Department of Chemistry, Zhejiang University, Hangzhou 310027, People's Republic of China

Complete contact information is available at:

<https://pubs.acs.org/doi/10.1021/acs.chemmater.0c00615>

Notes

The authors declare no competing financial interest.

ACKNOWLEDGMENTS

F.H. thanks the National Natural Science Foundation of China (21620102006) for financial support.

REFERENCES

- (1) Fujita, M.; Tominaga, M.; Hori, A.; Therrien, B. Coordination Assemblies from a Pd(II)-Cornered Square Complex. *Acc. Chem. Res.* **2005**, *38*, 369–378.
- (2) Cook, T. R.; Zheng, Y.-R.; Stang, P. J. Metal–Organic Frameworks and Self-Assembled Supramolecular Coordination Complexes: Comparing and Contrasting the Design, Synthesis, and Functionality of Metal–Organic Materials. *Chem. Rev.* **2013**, *113*, 734–777.
- (3) Chan, A. K.-W.; Lam, W. H.; Tanaka, Y.; Wong, K. M.-C.; Yam, V. W. W. Multiaddressable Molecular Rectangles with Reversible Host–Guest Interactions: Modulation of pH-Controlled Guest Release and Capture. *Proc. Natl. Acad. Sci. U. S. A.* **2015**, *112*, 690–695.
- (4) Zhou, J.; Zhang, Y.; Yu, G.; Crawley, M. R.; Fulong, C. R. P.; Friedman, A. E.; Sengupta, S.; Sun, J.; Li, Q.; Huang, F.; Cook, T. R. Highly Emissive Self-Assembled BODIPY-Platinum Supramolecular Triangles. *J. Am. Chem. Soc.* **2018**, *140*, 7730–7736.
- (5) Zhang, D.; Ronson, T. K.; Mosquera, J.; Martinez, A.; Nitschke, J. R. Selective Anion Extraction and Recovery Using a Fe^{II}₄L₄ Cage. *Angew. Chem., Int. Ed.* **2018**, *57*, 3717–3721.
- (6) Yu, G.; Yu, S.; Saha, M. L.; Zhou, J.; Cook, T. R.; Yung, B. C.; Chen, J.; Mao, Z.; Zhang, F.; Zhou, Z.; Liu, Y.; Shao, L.; Wang, S.; Gao, C.; Huang, F.; Stang, P. J.; Chen, X. A Discrete Organoplatinum-

(II) Metallacage as a Multimodality Theranostic Platform for Cancer Photochemotherapy. *Nat. Commun.* **2018**, *9*, 4335.

(7) Yan, X.; Wei, P.; Liu, Y.; Wang, M.; Chen, C.; Zhao, J.; Li, G.; Saha, M. L.; Zhou, Z.; An, Z.; Li, X.; Stang, P. J. Endo- and exo-Functionalized Tetraphenylethylene $M_{12}L_{24}$ Nanospheres: Fluorescence Emission inside a Confined Space. *J. Am. Chem. Soc.* **2019**, *141*, 9673–9679.

(8) Giansante, C.; Ceroni, P.; Balzani, V.; Vögtle, F. Self-Assembly of a Light-Harvesting Antenna Formed by a Dendrimer, a Ru^{II} Complex, and a Nd^{III} Ion. *Angew. Chem., Int. Ed.* **2008**, *47*, 5422–5425.

(9) Oliveri, C. G.; Ulmann, P. A.; Wiester, M. J.; Mirkin, C. A. Heteroligated Supramolecular Coordination Complexes Formed via the Halide-Induced Ligand Rearrangement Reaction. *Acc. Chem. Res.* **2008**, *41*, 1618–1629.

(10) Frischmann, P. D.; Kunz, V.; Würthner, F. Bright Fluorescence and Host–Guest Sensing with a Nanoscale $M_{4}L_{6}$ Tetrahedron Accessed by Self-Assembly of Zinc–Imine Chelate Vertices and Perylene Bisimide Edges. *Angew. Chem., Int. Ed.* **2015**, *54*, 7285–7289.

(11) Zheng, Y.-R.; Suntharalingam, K.; Johnstone, T. C.; Lippard, S. J. Encapsulation of Pt(IV) Prodrugs within a Pt(II) Cage for Drug Delivery. *Chem. Sci.* **2015**, *6*, 1189–1193.

(12) Cook, T. R.; Stang, P. J. Recent Developments in the Preparation and Chemistry of Metallacycles and Metallacages via Coordination. *Chem. Rev.* **2015**, *115*, 7001–7045.

(13) Zheng, W.; Chen, L.-J.; Yang, G.; Sun, B.; Wang, X.; Jiang, B.; Yin, G.-Q.; Zhang, L.; Li, X.; Liu, M.; Chen, G.; Yang, H.-B. Construction of Smart Supramolecular Polymeric Hydrogels Cross-linked by Discrete Organoplatinum(II) Metallacycles via Post-Assembly Polymerization. *J. Am. Chem. Soc.* **2016**, *138*, 4927–4937.

(14) Samanta, S. K.; Moncelet, D.; Briken, V.; Isaacs, L. Metal-Organic Polyhedron Capped with Cucurbit[8]uril Delivers Doxorubicin to Cancer Cells. *J. Am. Chem. Soc.* **2016**, *138*, 14488–14496.

(15) Zheng, W.; Yang, G.; Shao, N.; Chen, L.-J.; Ou, B.; Jiang, S.-T.; Chen, G.; Yang, H.-B. CO_2 Stimuli-Responsive, Injectable Block Copolymer Hydrogels Cross-Linked by Discrete Organoplatinum(II) Metallacycles via Stepwise Post-Assembly Polymerization. *J. Am. Chem. Soc.* **2017**, *139*, 13811–13820.

(16) Li, Q.-L.; Sun, Y.; Sun, Y.-L.; Wen, J.; Zhou, Y.; Bing, Q.-M.; Isaacs, L. D.; Jin, Y.; Gao, H.; Yang, Y.-W. Mesoporous Silica Nanoparticles Coated by Layer-by-Layer Self-Assembly Using Cucurbit[7]uril for in Vitro and in Vivo Anticancer Drug Release. *Chem. Mater.* **2014**, *26*, 6418–6431.

(17) Guo, D.-S.; Liu, Y. Supramolecular Chemistry of *p*-Sulfonatocalix[*n*]arenes and Its Biological Applications. *Acc. Chem. Res.* **2014**, *47*, 1925–1934.

(18) Tian, Y.-K.; Shi, Y.-G.; Yang, Z.-S.; Wang, F. Responsive Supramolecular Polymers Based on the Bis[alkynylplatinum(II)] Terpyridine Molecular Tweezer/Arene Recognition Motif. *Angew. Chem., Int. Ed.* **2014**, *53*, 6090–6094.

(19) Yu, G.; Cook, T. R.; Li, Y.; Yan, X.; Wu, D.; Shao, L.; Shen, J.; Tang, G.; Huang, F.; Chen, X.; Stang, P. J. Tetraphenylethene-Based Highly Emissive Metallacage as a Component of Theranostic Supramolecular Nanoparticles. *Proc. Natl. Acad. Sci. U. S. A.* **2016**, *113*, 13720–13725.

(20) Hu, X.-Y.; Liu, X.; Zhang, W.; Qin, S.; Yao, C.; Li, Y.; Cao, D.; Peng, L.; Wang, L. Controllable Construction of Biocompatible Supramolecular Micelles and Vesicles by Water-Soluble Phosphate Pillar[5,6]arenes for Selective Anti-Cancer Drug Delivery. *Chem. Mater.* **2016**, *28*, 3778–3788.

(21) Zhao, Y. Emerging Applications of Metal–Organic Frameworks and Covalent Organic Frameworks. *Chem. Mater.* **2016**, *28*, 8079–8081.

(22) Zhou, J.; Yu, G.; Huang, F. Supramolecular Chemotherapy Based on Host–Guest Molecular Recognition: a Novel Strategy in the Battle against Cancer with a Bright Future. *Chem. Soc. Rev.* **2017**, *46*, 7021–7053.

(23) Zhang, Q.; Zhang, F.; Chen, Y.; Dou, Y.; Tao, H.; Zhang, D.; Wang, R.; Li, X.; Zhang, J. Structure–Property Correlations of

Reactive Oxygen Species-Responsive and Hydrogen Peroxide-Eliminating Materials with Anti-Oxidant and Anti-Inflammatory Activities. *Chem. Mater.* **2017**, *29*, 8221–8238.

(24) Li, B.; Meng, Z.; Li, Q.; Huang, X.; Kang, Z.; Dong, H.; Chen, J.; Sun, J.; Dong, Y.; Li, J.; Jia, X.; Sessler, J. L.; Meng, Q.; Li, C. A pH Responsive Complexation-Based Drug Delivery System for Oxaliplatin. *Chem. Sci.* **2017**, *8*, 4458–4464.

(25) Brendel, J. C.; Sanchis, J.; Catrouillet, S.; Czuba, E.; Chen, M. Z.; Long, B. M.; Nowell, C.; Johnston, A.; Jolliffe, K. A.; Perrier, S. Secondary Self-Assembly of Supramolecular Nanotubes into Tubosomes and Their Activity on Cells. *Angew. Chem., Int. Ed.* **2018**, *57*, 16678–16682.

(26) Zhang, Z.; Zhao, Z.; Hou, Y.; Wang, H.; Li, X.; He, G.; Zhang, M. Aqueous Platinum(II)-Cage-Based Light-Harvesting System for Photocatalytic Cross-Coupling Hydrogen Evolution Reaction. *Angew. Chem., Int. Ed.* **2019**, *58*, 8862–8866.

(27) Yu, G.; Zhu, B.; Shao, L.; Zhou, J.; Saha, M. L.; Shi, B.; Zhang, Z.; Hong, T.; Li, S.; Chen, X.; Stang, P. J. Host–Guest Complexation-Mediated Codelivery of Anticancer Drug and Photosensitizer for Cancer Photochemotherapy. *Proc. Natl. Acad. Sci. U. S. A.* **2019**, *116*, 6618–6623.

(28) Zhou, J.; Yu, G.; Li, Q.; Wang, M.; Huang, F. Separation of Benzene and Cyclohexane by Nonporous Adaptive Crystals of a Hybrid[3]arene. *J. Am. Chem. Soc.* **2020**, *142*, 2228–2232.

(29) Han, M.; Engelhard, D. M.; Clever, G. H. Self-Assembled Coordination Cages Based on Banana-Shaped Ligands. *Chem. Soc. Rev.* **2014**, *43*, 1848–1860.

(30) Chen, L.-J.; Yang, H.-B.; Shionoya, M. Chiral Metallosupramolecular Architectures. *Chem. Soc. Rev.* **2017**, *46*, 2555–2576.

(31) Howlader, P.; Mondal, B.; Purba, P. C.; Zangrando, E.; Mukherjee, P. S. Self-Assembled Pd(II) Barrels as Containers for Transient Merocyanine Form and Reverse Thermochromism of Spiropyran. *J. Am. Chem. Soc.* **2018**, *140*, 7952–7960.

(32) Zheng, Y.-R.; Lan, W.-J.; Wang, M.; Cook, T. R.; Stang, P. J. Designed Post-Self-Assembly Structural and Functional Modifications of a Truncated Tetrahedron. *J. Am. Chem. Soc.* **2011**, *133*, 17045–17055.

(33) Roberts, D. A.; Pilgrim, B. S.; Nitschke, J. R. Covalent Post-Assembly Modification in Metallosupramolecular Chemistry. *Chem. Soc. Rev.* **2018**, *47*, 626–644.

(34) Gody, G.; Rossner, C.; Moraes, J.; Vana, P.; Maschmeyer, T.; Perrier, S. One-Pot RAFT/“Click” Chemistry via Isocyanates: Efficient Synthesis of α -End-Functionalized Polymers. *J. Am. Chem. Soc.* **2012**, *134*, 12596–12603.

(35) Acharyya, K.; Mukherjee, P. S. Organic Imine Cages: Molecular Marriage and Applications. *Angew. Chem., Int. Ed.* **2019**, *58*, 8640–8653.

(36) Leigh, D. A.; Lusby, P. J.; McBurney, R. T.; Morelli, A.; Slawin, A. M. Z.; Thomson, A. R.; Walker, D. B. Getting Harder: Cobalt(III)-Template Synthesis of Catenanes and Rotaxanes. *J. Am. Chem. Soc.* **2009**, *131*, 3762–3771.

(37) Feringa, B. L. The Art of Building Small: From Molecular Switches to Motors (Nobel Lecture). *Angew. Chem., Int. Ed.* **2017**, *56*, 11060–11078.

(38) Sauvage, J.-P. From Chemical Topology to Molecular Machines (Nobel Lecture). *Angew. Chem., Int. Ed.* **2017**, *56*, 11080–11093.

(39) Stoddart, J. F. Mechanically Interlocked Molecules (MIMs)—Molecular Shuttles, Switches, and Machines (Nobel Lecture). *Angew. Chem., Int. Ed.* **2017**, *56*, 11094–11125.

(40) Price, T. L., Jr.; Gibson, H. W. Supramolecular Pseudorotaxane Polymers from Biscryptands and Bisparaquats. *J. Am. Chem. Soc.* **2018**, *140*, 4455–4465.

(41) Li, J.-R.; Sculley, J.; Zhou, H.-C. Metal–Organic Frameworks for Separations. *Chem. Rev.* **2012**, *112*, 869–932.

(42) Furukawa, H.; Cordova, K. E.; O’Keeffe, M.; Yaghi, O. M. The Chemistry and Applications of Metal–Organic Frameworks. *Science* **2013**, *341*, 1230444.

- (43) Aida, T.; Meijer, E. W.; Stupp, S. I. Functional Supramolecular Polymers. *Science* **2012**, *335*, 813–817.
- (44) Matyjaszewski, K.; Xia, J. Atom Transfer Radical Polymerization. *Chem. Rev.* **2001**, *101*, 2921–2990.
- (45) Cook, T. R.; Vajpayee, V.; Lee, M. H.; Stang, P. J.; Chi, K.-W. Biomedical and Biochemical Applications of Self-Assembled Metallacycles and Metallacages. *Acc. Chem. Res.* **2013**, *46*, 2464–2474.
- (46) Yu, G.; Zhang, M.; Saha, M. L.; Mao, Z.; Chen, J.; Yao, Y.; Zhou, Z.; Liu, Y.; Gao, C.; Huang, F.; Chen, X.; Stang, P. J. Antitumor Activity of a Unique Polymer That Incorporates a Fluorescent Self-Assembled Metallacycle. *J. Am. Chem. Soc.* **2017**, *139*, 15940–15949.
- (47) Elsabahy, M.; Heo, G. S.; Lim, S.-M.; Sun, G.; Wooley, K. L. Polymeric Nanostructures for Imaging and Therapy. *Chem. Rev.* **2015**, *115*, 10967–11011.
- (48) Datta, S.; Saha, M. L.; Stang, P. J. Hierarchical Assemblies of Supramolecular Coordination Complexes. *Acc. Chem. Res.* **2018**, *51*, 2047–2063.
- (49) Sepehrpour, H.; Fu, W.; Sun, Y.; Stang, P. J. Biomedically Relevant Self-Assembled Metallacycles and Metallacages. *J. Am. Chem. Soc.* **2019**, *141*, 14005–14020.
- (50) Ge, Z.; Liu, S. Functional Block Copolymer Assemblies Responsive to Tumor and Intracellular Microenvironments for Site-Specific Drug Delivery and Enhanced Imaging Performance. *Chem. Soc. Rev.* **2013**, *42*, 7289–7325.
- (51) Lu, Y.; Aimetti, A. A.; Langer, R.; Gu, Z. Bioresponsive Materials. *Nat. Rev. Mater.* **2017**, *2*, 16075.
- (52) Chen, H.; Zhang, W.; Zhu, G.; Xie, J.; Chen, X. Rethinking Cancer Nanotheranostics. *Nat. Rev. Mater.* **2017**, *2*, 17024.
- (53) Fu, X.; Hosta-Rigau, L.; Chandrawati, R.; Cui, J. Multi-Stimuli-Responsive Polymer Particles, Films, and Hydrogels for Drug Delivery. *Chem.* **2018**, *4*, 2084–2107.
- (54) Shi, J.; Kantoff, P. W.; Wooster, R.; Farokhzad, O. C. Cancer Nanomedicine: Progress, Challenges and Opportunities. *Nat. Rev. Cancer* **2017**, *17*, 20–37.
- (55) Sun, Q.; Zhou, Z.; Qiu, N.; Shen, Y. Rational Design of Cancer Nanomedicine: Nanoproperty Integration and Synchronization. *Adv. Mater.* **2017**, *29*, 1606628.
- (56) Deng, Z.; Qian, Y.; Yu, Y.; Liu, G.; Hu, J.; Zhang, G.; Liu, S. Engineering Intracellular Delivery Nanocarriers and Nanoreactors from Oxidation-Responsive Polymersomes via Synchronized Bilayer Cross-Linking and Permeabilizing Inside Live Cells. *J. Am. Chem. Soc.* **2016**, *138*, 10452–10466.
- (57) Yin, W.; Li, J.; Ke, W.; Zha, Z.; Ge, Z. Integrated Nanoparticles to Synergistically Elevate Tumor Oxidative Stress and Suppress Antioxidative Capability for Amplified Oxidation Therapy. *ACS Appl. Mater. Interfaces* **2017**, *9*, 29538–29546.
- (58) Noh, J.; Kwon, B.; Han, E.; Park, M.; Yang, W.; Cho, W.; Yoo, W.; Khang, G.; Lee, D. Amplification of Oxidative Stress by a Dual Stimuli-Responsive Hybrid Drug Enhances Cancer Cell Death. *Nat. Commun.* **2015**, *6*, 6907.
- (59) Li, J.; Dirisala, A.; Ge, Z.; Wang, Y.; Yin, W.; Ke, W.; Toh, K.; Xie, J.; Matsumoto, Y.; Anraku, Y.; Osada, K.; Kataoka, K. Therapeutic Vesicular Nanoreactors with Tumor-Specific Activation and Self-Destruction for Synergistic Tumor Ablation. *Angew. Chem., Int. Ed.* **2017**, *56*, 14025–14030.
- (60) Chen, Q.; Espey, M. G.; Krishna, M. C.; Mitchell, J. B.; Corpe, C. P.; Buettner, G. R.; Shacter, E.; Levine, M. Pharmacologic Ascorbic Acid Concentrations Selectively Kill Cancer Cells: Action as a Pro-drug to Deliver Hydrogen Peroxide to Tissues. *Proc. Natl. Acad. Sci. U. S. A.* **2005**, *102*, 13604–13609.
- (61) Li, J.; Ke, W.; Wang, L.; Huang, M.; Yin, W.; Zhang, P.; Chen, Q.; Ge, Z. Self-Sufficing H₂O₂-Responsive Nanocarriers through Tumor-Specific H₂O₂ Production for Synergistic Oxidation-Chemotherapy. *J. Controlled Release* **2016**, *225*, 64–74.
- (62) Peer, D.; Karp, J. M.; Hong, S.; Farokhzad, O. C.; Margalit, R.; Langer, R. Nanocarriers as an Emerging Platform for Cancer Therapy. *Nat. Nanotechnol.* **2007**, *2*, 751–760.
- (63) Nakamura, Y.; Mochida, A.; Choyke, P. L.; Kobayashi, H. Nanodrug Delivery: Is the Enhanced Permeability and Retention Effect Sufficient for Curing Cancer? *Bioconjugate Chem.* **2016**, *27*, 2225–2238.
- (64) Knop, K.; Hoogenboom, R.; Fischer, D.; Schubert, U. S. Poly(ethylene glycol) in Drug Delivery: Pros and Cons as Well as Potential Alternatives. *Angew. Chem., Int. Ed.* **2010**, *49*, 6288–6308.